Supporting Material

Multi-motor transport in a system of active and inactive kinesin-1 motors

Lara Scharrel[1, 2, *], Rui Ma[3, *], René Schneider[1,4], Frank Jülicher[3, †], Stefan Diez[1, 2, †]

[1] B CUBE - Center for Molecular Bioengineering, Technische Universität Dresden, Germany
[2] Max Planck Institute of Cell Biology and Genetics, Dresden, Germany
[3] Max Planck Institute for the Physics of Complex Systems, Dresden, Germany
[4] current address: Max Planck Institute of Molecular Plant Physiology, Potsdam-Golm, Germany

[*] equal contribution, [†] correspondence to: julicher@pks.mpg.de and diez@bcube-dresden.de

---

Gliding velocities and number of data points for experiment and simulation

N_a/N	0.3	0.4	0.5	0.6	0.7	0.8	0.9	1.0
Experiment								
Gaussian fit (nm/s)	4±20	2±32	2±67	7±20 181±191	17±20 478±202	697±108	764±74	773±48
Mean ± s.d. (nm/s)	4±21	4±38	5±82	53±137	387±236	650±169	737±125	766±79
Mean length± s.d. (µm)	4.7±3.4	4.8±3.8	4.3±2.6	4.9±3.7	5.6±3.9	5.2±4.4	5.3±3.5	6.9±4.7
Number of data points	*10022*	*23649*	*13034*	*20722*	*28394*	*22537*	*22966*	*27964*
Simulation								
Gaussian fit (nm/s)	0±9	0±10	1±12	2±14	12±29 568±75	672±49	732±36	773±28
Mean ± s.d. (nm/s)	0±0	0±0	1±0	24±54	395±117	645±65	721±33	766±23
No of data points	200000	200000	200000	200000	200000	200000	200000	200000

Supporting Table T1: Microtubule gliding velocities, length of microtubules and number of data points (number of instantaneous velocities of all filaments) for experiment and simulation. Gaussian fit represents the coefficients of the single or double Gaussian fit to the histograms ± standard deviation. Mean±s.d. (nm/s) gives the arithmetic mean ± standard deviation of all microtubule velocities (see Figure 4). Mean length ±s.d. (µm) gives the arithmetic mean ± standard deviation of all microtubule lengths.

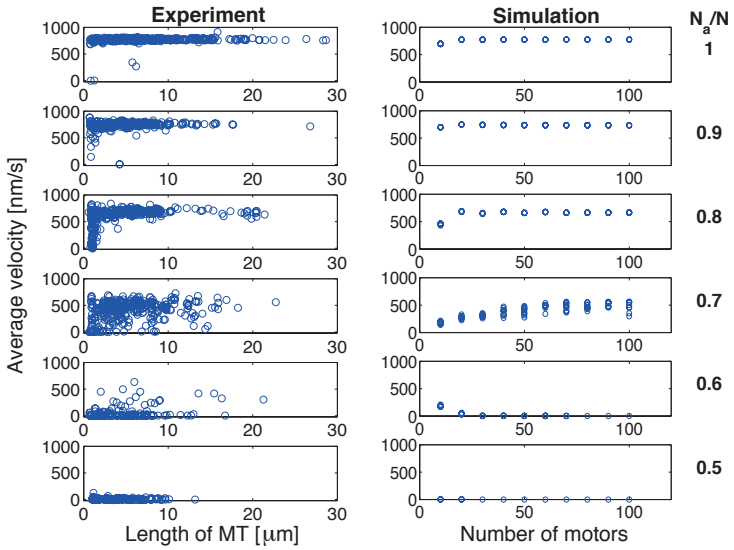

Figure S1: Length dependence of the average velocity of single microtubules for different N_a/N for experiment (A) and simulation (B). We found in the experiments that shorter microtubules (< 5 µm) slow down already at higher N_a/N (N_a/N=0.9) compared to longer microtubules. In the simulation microtubules with only 10 motors also slowed down already at higher N_a/N, but not as significantly as in the experiment. In addition, in the simulation at N_a/N =0.6 microtubules with only 10 motors exhibit a faster average velocity than longer ones, which wasn't observed in the experiment. A difference in length of the microtubule corresponds to a different number of total motors acting on the microtubule. For shorter microtubules (i.e. smaller numbers of motors) fluctuations by the local variations of active and inactive motors get more apparent and lead to a change in the average velocity.

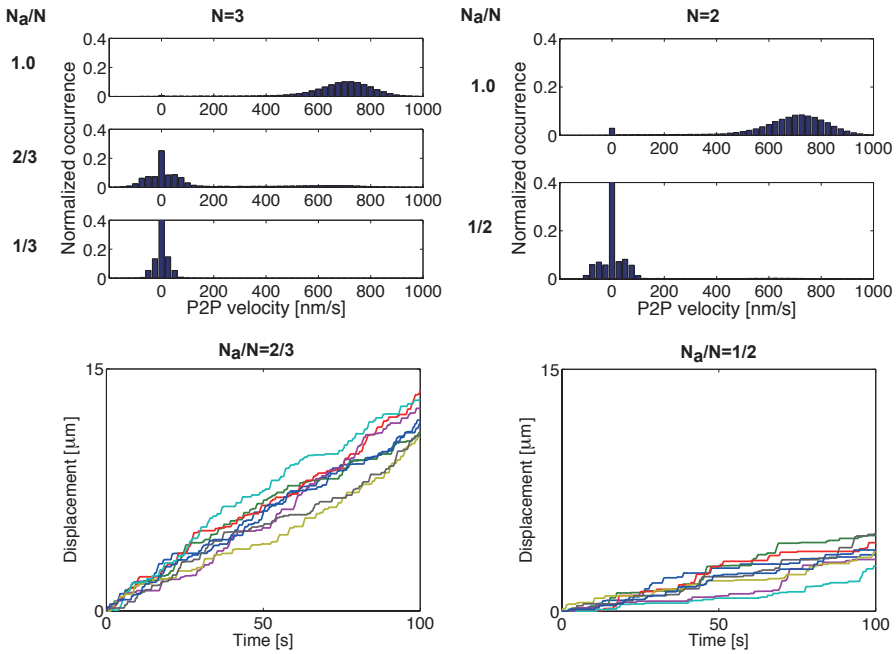

Figure S2: Normalized histograms (bin size 25 nm/s) of gliding microtubules for different ratios of N_a/N and trajectories of microtubules. The results are obtained from 200 simulations with a fixed number of motors $N = 3$ (left column), and $N = 2$ (right column). Parameters are the same as in Figure 2B. If two out of three (or one out of two) motors are active, coexistence of a broad distribution of slow motility around 0 nm/s with a long but low tail of fast motility is observed. With one out of three motors active, only slow motility is observed.

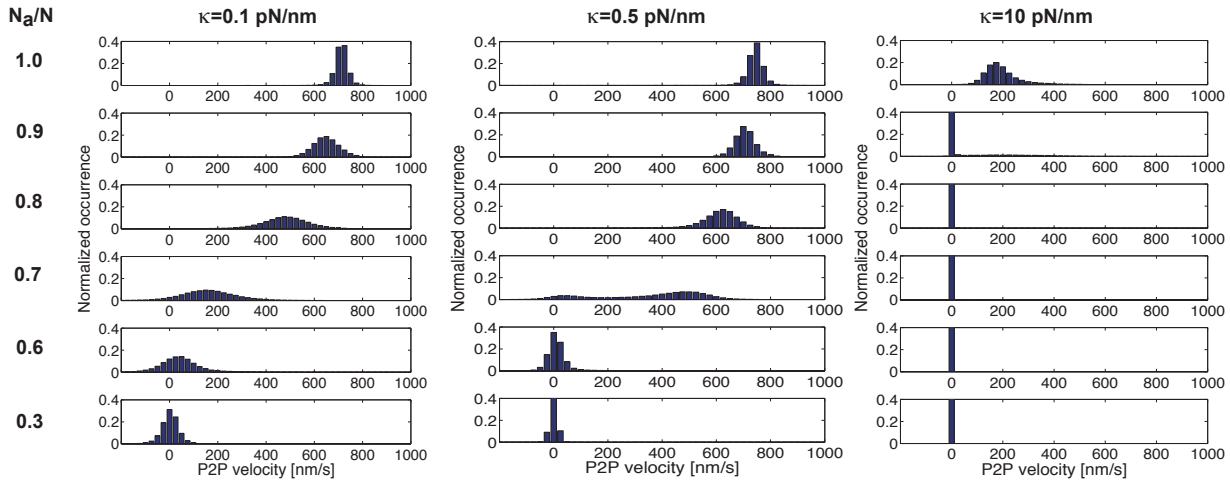

Figure S3: Normalized histograms (bin size 25 nm/s) of gliding microtubules for different ratios of N_a/N. The results are obtained from 200 simulations. Parameters are the same as in Figure 2B except that the motor stiffness is 0.1 pN/nm, 0.5 pN/nm and 10 pN/nm (from left to right). At a low motor stiffness of $\kappa = 0.1$ pN/nm the transition from fast to slow motility is smooth and no coexistence region is observed. At a motor stiffness of $\kappa = 0.5$ pN/nm coexistence of fast to slow motility is observed at $N_a/N = 0.7$, but the transition is smoother than compared to simulations using $\kappa = 1$ pN/nm (Figure 2B). At a high motor stiffness of $\kappa = 10$ pN/nm gliding is only observed at $N_a/N = 1$ and 0.9, as the stiff linkers stall the gliding microtubule immediately.

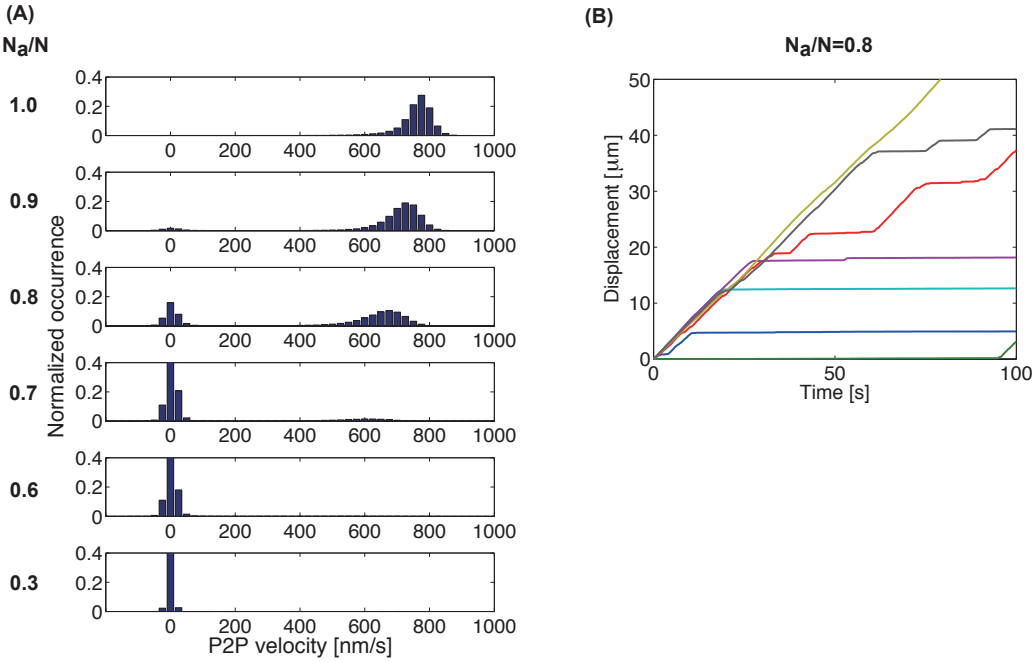

Figure S4: (A) Normalized histograms (bin size 25 nm/s) of gliding microtubules for different ratios of N_a/N. The results are obtained from 200 simulations in which motors are randomly distributed ($P(l) = \alpha\, e^{-\alpha x}$ with an average distance $< l >= {}^{1}/_{\alpha} = 100\, nm$) on the substrate and active and inactive motors are randomly mixed. (B) Simulated trajectories of microtubules for $N_a/N = 0.8$ where fast and slow motility coexist. Parameters are the same as in Figure 2B. Compared to Figure 2B, acquired from simulations in which the distribution of motors and the ratio of active per total motors in a simulation run was constant, the main region of coexistence shifted from $N_a/N = 0.7$ to $N_a/N = 0.8$, and the width of the velocity distribution increased.

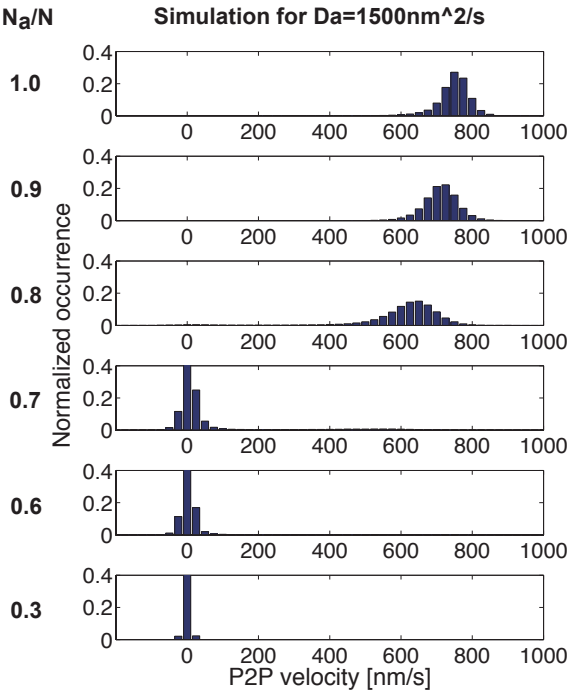

Figure S5: Normalized histograms (bin size 25 nm/s) of gliding microtubules for different ratios of N_a/N. The results are obtained from 200 simulations with $D_a = 1500\ nm^2/s$ (corresponding to a randomness factor $r = 0.5$ as obtained in single molecule experiments, other parameters the same as in Figure 2B). We found that the coexistence of fast and slow motility at $N_a/N = 0.7$ is less pronounced than compared to histograms acquired from simulations using $D_a = 1000\ nm^2/s$ (Figure 2B). The rather low randomness parameter, fitting best our experimental data, might result from collective effects of multiple motors or the short length of the truncated kinesins used.

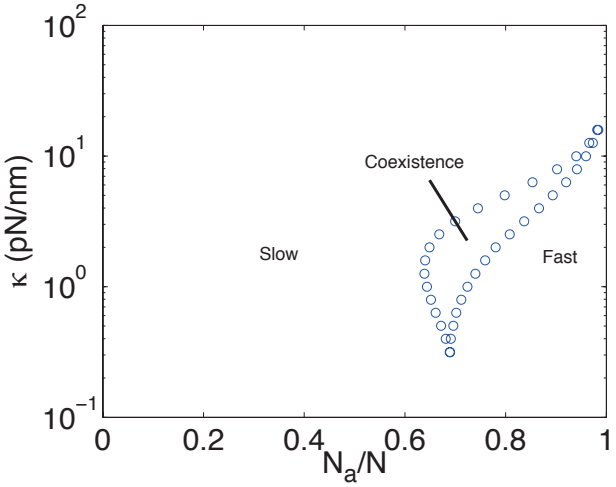

Figure S6: Phase diagram parameterized with N_a/N and the stiffness of motors κ for the mean field approach. Blue circles represent the lower and upper critical ratios, which confine the region of coexistence of fast and slow motility. Other parameters are the same as in Figure 2B. Coexistence of fast and slow motility exists for $0.3\ pN/nm < \kappa <$ 10 pN/nm and is shifted to higher N_a/N for increased κ.

Captions for Supporting Movies M1 – M3:

Movies M1-M3 show different motility regimes of gliding microtubules observed at three ratios of N_a/N. The examples show fast gliding at maximum velocity (for $N_a/N = 1$, movie M1), bistable movement with phases of fast and slow motility (for $N_a/N = 0.7$, movie M2) and stopping (for $N_a/N = 0.3$, movie M3).